

FILAMENTARY LARGE SCALE STRUCTURE TRACED BY SIX Ly α BLOBS AT $Z = 2.3$

DAWN K. ERB¹, MILAN BOGOSAVLJEVIĆ², AND CHARLES C. STEIDEL³

Accepted for publication in ApJL

ABSTRACT

Extended nebulae of Ly α emission (“Ly α blobs”) are known to be associated with overdense regions at high redshift. Here we present six large Ly α blobs in a previously known protocluster with galaxy overdensity $\delta \sim 7$ at $z = 2.3$; this is the richest field of giant Ly α blobs detected to date. The blobs have linear sizes of $\gtrsim 100$ kpc and Ly α luminosities of $\sim 10^{43}$ erg s⁻¹. The positions of the blobs define two linear filaments with an extent of at least 12 comoving Mpc; these filaments intersect at the center of one of the blobs. Measurement of the position angles of the blobs indicates that five of the six are aligned with these filaments to within $\sim 10^\circ$, suggesting a connection between the physical processes powering extended Ly α emission and those driving structure on larger scales.

Subject headings: galaxies: evolution—galaxies: formation—galaxies: high-redshift—large-scale structure of universe

1. INTRODUCTION

Large, extended regions of Ly α emission, also known as Ly α blobs, have been most commonly found in overdense regions at redshifts $z \sim 2$ to $z \sim 3$. These objects have sizes of ~ 50 – 100 kpc, Ly α luminosities of $\sim 10^{43}$ – 10^{44} erg s⁻¹, and, in contrast to the large Ly α nebulae surrounding some high redshift radio galaxies (e.g. McCarthy et al. 1987), do not have obvious sources for their strong emission. Since the first two such blobs were found in an overdensity at $z = 3.1$ (Steidel et al. 2000), additional blobs have been found in the same region (Matsuda et al. 2004, 2005), in other dense regions (Palunas et al. 2004; Prescott et al. 2008; Matsuda et al. 2009), and, less frequently, in the field (Yang et al. 2009; Matsuda et al. 2011). Lower redshift ($z = 0.8$) searches for Ly α blobs have so far found none (Keel et al. 2009), suggesting that the blobs are a high redshift phenomenon.

While the blobs’ preferential location in overdense environments indicates an association with massive galaxy formation, the mechanism which powers the Ly α emission remains unclear. Proposed sources have generally fallen into two categories: cooling radiation from cold streams of gas accreting onto galaxies (e.g. Haiman et al. 2000; Dijkstra & Loeb 2009; Goerdt et al. 2010), and photoionization and/or mechanical feedback from starbursts or AGN (e.g. Taniguchi & Shioya 2000; Geach et al. 2009). Supporting evidence for the cooling flow scenario comes from those blobs lacking any visible power source, in both the optical and infrared (Nilsson et al. 2006; Smith et al. 2008), while the significant number of blobs containing massive, luminous galaxies or AGN suggests that internal heating plays an important role (Geach et al. 2009; Colbert et al. 2011).

Most recently, attention has been directed to the effects of Ly α radiative transfer and resonant scattering, sug-

gesting that cooling alone is insufficient to account for the observed luminosity (Faucher-Giguère et al. 2010). Also recently, stacking of narrowband Ly α images of galaxies at $z \sim 2$ – 3 has revealed extended, diffuse Ly α halos, suggesting that such emission is a general property of high redshift galaxies, and that the distinction between a galaxy and a Ly α blob may simply be a matter of the surface brightness threshold of the observation (Steidel et al. 2011). The typical sizes of these extended halos (~ 80 kpc) are comparable in extent to the metals and H I detected in absorption near galaxies (Steidel et al. 2010), implying that the Ly α emission is due to resonant scattering of photons produced in galactic H II regions by outflowing gas. Similarly, Zheng et al. (2010) predict that resonant scattering will produce extended Ly α halos around galaxies at high redshift, resulting in a coupling between the observed Ly α emission and the properties of the circumgalactic and intergalactic media on larger scales.

In this Letter we present six large Ly α blobs discovered in the course of a narrowband imaging survey for Ly α emission associated with a known protocluster. The $z = 2.300 \pm 0.015$ HS 1700+643 protocluster (Steidel et al. 2005) has a redshift-space galaxy overdensity $\delta \sim 7$ and a mass scale of $\sim 1.4 \times 10^{15} M_\odot$, indicating that it will evolve into a rich galaxy cluster by $z = 0$. Galaxies in the overdensity have typical masses and ages ~ 2 times larger than comparably selected field galaxies, while an analysis of *HST* ACS images finds no significant morphological differences between protocluster and field galaxies (Peter et al. 2007). The protocluster has also been the target of a 200-ks *Chandra*/ACIS-I observation, which indicated an excess of AGN activity relative to a similarly selected field sample (Digby-North et al. 2010).

We use a cosmology with $H_0 = 70$ km s⁻¹ Mpc⁻¹, $\Omega_m = 0.3$, and $\Omega_\Lambda = 0.7$.

2. DATA

The Ly α blobs were detected in a deep, narrowband image centered at 4010 Å, using the LFC Wide-Field Imager on the Hale 200-inch telescope at Palomar Observatory and a custom filter with FWHM = 90 Å designed

¹ Department of Physics, University of Wisconsin Milwaukee, Milwaukee, WI, 53211; dawn@gravity.phys.uwm.edu

² Astronomical Observatory, Volgina 7, 11060 Belgrade, Serbia; mbogosavljevic@aob.rs

³ Department of Astronomy, California Institute of Technology, MS 249–17, Pasadena, CA 91125; ccs@astro.caltech.edu

to match Ly α emission at $z = 2.3$. The 22.3 hr exposure has a 3σ depth of $NB \sim 27.8$ mag arcsec $^{-2}$ and an area of 219 arcmin 2 . The observations, data reduction and resulting catalog of Ly α emitters are described in detail elsewhere (Erb et al., in prep). In brief, individual exposures were 1800 s, with sky subtraction using the IRAF task “insurfit” and masking of satellite tracks done on individual frames. The individual frames were then combined and matched to a continuum image created via a linear combination of U_n and G images (the peak transmission of the 4010 Å filter lies directly between the U_n and G bands). Final background subtraction and object detection was done with SExtractor, and the resulting final image and background image were carefully examined for residual artifacts which could affect the blob profiles. Spectroscopic followup of portions of the blobs was carried out with the Low Resolution Imaging Spectrometer (LRIS) on the Keck I telescope, following procedures described by Steidel et al. (2004).

The HS 1700+64 field has been the subject of extensive deep, multiwavelength imaging: near-IR J and K_s observations are presented by Erb et al. (2006), *Spitzer* IRAC observations in all four channels by Barmby et al. (2004) and Shapley et al. (2005), and 24 μ m *Spitzer* MIPS observations by Reddy et al. (2010). This imaging covers a smaller area than the optical and narrowband images; two of the blobs presented here (Blobs 5 and 6) are not covered by the IR observations.

We identify rest-frame UV-selected protocluster galaxies and candidates as described by Steidel et al. (2004, 2005), and select Distant Red Galaxies (DRGs) with $J - K_s > 2.3$ (Franx et al. 2003). The DRGs have a broad redshift range, from $z \sim 1.2$ to $z \sim 3.7$ with a median of $z \sim 2.7$, though large spectroscopic samples have been difficult to obtain because of their optical faintness (Wuyts et al. 2009). Additional followup of the spectroscopic sample indicates that the DRGs are massive and divided between dusty galaxies with high star formation rates and compact, quiescent galaxies (Kriek et al. 2009). The catalog of DRGs is largely complementary to the UV-selected galaxy catalog, with relatively small overlap of $\sim 12\%$ between the two selection methods (Reddy et al. 2005).

3. SIX Ly α BLOBS AT $Z = 2.3$

The narrowband image contains six regions of extended Ly α emission, classified as “blobs” based on an isophotal size of at least 50 arcsec 2 with a 1σ surface brightness limit of $NB = 29$ mag arcsec $^{-2}$ or 1.5×10^{-18} erg s $^{-1}$ cm $^{-2}$ arcsec $^{-2}$. With this threshold, the blobs have areas of ~ 50 –130 arcsec 2 and luminosities of $\sim 10^{43}$ erg s $^{-1}$. Because of the irregular shape of the blobs, linear size measurements are difficult. In order to estimate the blobs’ linear extent, elongation and position angle, we fit an ellipse to the largest 1.5×10^{-18} erg s $^{-1}$ cm $^{-2}$ arcsec $^{-2}$ contour. The major axis of the ellipse then approximates the size of the blob, and the ellipticity and position angle measure its elongation and orientation. Properties of the blobs are given in Table 1, and images of the blobs with overlaid contours and the best-fit ellipses are shown in Figure 1.

3.1. Space Density

Given the 219 arcmin 2 area and filter bandwidth sensitive to Ly α emission from $z = 2.24$ to $z = 2.36$, the effective survey volume is $V \simeq 10^5$ comoving Mpc 3 . We therefore estimate the space density of blobs in the protocluster to be $n \sim 6 \times 10^{-5}$ Mpc $^{-3}$. In a blind, field survey at the same redshift and to a similar luminosity threshold (though allowing a smaller total blob area), Yang et al. (2009) found a blob density of 2.5×10^{-6} Mpc $^{-3}$, a factor of 24 lower than the density in the HS 1700+64 protocluster. Even when accounting for the protocluster’s $\delta \sim 7$ galaxy density enhancement, the blob density remains higher by a factor of ~ 3 . Yang et al. (2009) reached a similar conclusion when comparing their observed blob density with that of the $z = 3.1$ overdensity in SSA22 (Matsuda et al. 2004). Our results therefore confirm earlier conclusions that Ly α blobs are more likely to be found in significantly overdense environments.

3.2. Redshifts

All of the blobs have been observed spectroscopically, several at more than one position, and confirmed to be associated with the $z = 2.3$ protocluster. Ly α emission redshifts range from $z = 2.267$ (Blob 5) to $z = 2.3082$ (Blob 2), corresponding to a velocity range of ~ 3700 km s $^{-1}$ (~ 1800 km s $^{-1}$ if Blob 5 is not included). There is no trend of redshift with blob position, and the range of blob redshifts is somewhat wider than the redshift range of the continuum-selected galaxy overdensity, $z = 2.300 \pm 0.015$ (Steidel et al. 2005).

3.3. Associations with Continuum-Selected Galaxies and Blob Kinematics

Most of the blobs are associated with continuum-selected galaxies confirmed or likely to lie in the protocluster; however, none are associated with known AGN, and none are detected in a deep *Chandra*/ACIS-I observation of the field (Digby-North et al. 2010). In this section we briefly describe the galaxies associated with each blob, and summarize what is known about the blobs’ kinematics.

Blob 1. The bright ($K_s = 19.2$), near-IR selected galaxy DRG64 lies near the center of Blob 1, between the two portions of the blob selected as Ly α emitters. DRG64 is also a bright 24 μ m source. The redshift of this galaxy is unknown, but given the low density of DRG candidates in the field the probability that this is a chance association is low. Ly α spectroscopy of the blob reveals extended emission at $z = 2.2929$, with velocity width $\sigma \sim 750$ km s $^{-1}$ and no significant velocity shift over the spatial extent of the emission.

Blob 2. Blob 2 is the only one of the six blobs not coincident with any UV- or IR-selected galaxy candidates. It is also the blob with the largest observed velocity gradient: spectroscopy of Ly α emission from three different portions of the blob reveals emission at $z = 2.3082$ at the core of the blob, $z = 2.3065$ at the northern of the two points marked as narrowband-selected Ly α emitters in Figure 1, and $z = 2.2930$ at the southern edge of the blob. Ly α emission from the edge of the blob is therefore blueshifted by ~ 1400 km s $^{-1}$ with respect to emission from the core of the blob 70 kpc away.

Blob 3. Blob 3 contains the UV-selected galaxy MD109, with a redshift from H α emission of $z = 2.2942$

TABLE 1
 Ly α BLOBS IN THE HS 1700+64 PROTOCLUSTER AT $z = 2.3$

| ID | RA (J2000) | Dec (J2000) | Area ^a (arcsec ²) | a^b (kpc) | e^c | PA ^d (deg) | W_0^e (Å) | $F_{\text{Ly}\alpha}^f$ (10^{-16} erg s ⁻¹ cm ⁻²) | $L_{\text{Ly}\alpha}$ (10^{43} erg s ⁻¹) |
|--------|---------------|----------------|---|----------------|-------|--------------------------|----------------|--|--|
| BLOB 1 | 17:00:46.99 | +64:15:43.5 | 105 | 151 | 0.50 | 97 | 126 | 4.6 | 1.8 |
| BLOB 2 | 17:00:56.56 | +64:13:27.2 | 61 | 149 | 0.56 | 156 | 125 | 3.5 | 1.4 |
| BLOB 3 | 17:01:04.16 | +64:12:11.8 | 128 | 125 | 0.12 | 140 | 129 | 6.6 | 2.6 |
| BLOB 4 | 17:01:32.53 | +64:14:16.4 | 95 | 137 | 0.22 | 110 | 158 | 5.6 | 2.2 |
| BLOB 5 | 17:01:41.31 | +64:14:03.3 | 53 | 103 | 0.19 | 99 | 71 | 3.2 | 1.2 |
| BLOB 6 | 17:01:54.54 | +64:13:39.6 | 78 | 119 | 0.17 | 9 | 121 | 3.5 | 1.4 |

^a Area of emission 1σ above sky in continuum-subtracted narrowband image.

^b Major axis diameter of ellipse fit to 1.5×10^{-18} erg s⁻¹ cm⁻² arcsec⁻² contour.

^c Ellipticity $e = 1 - b/a$ of best-fit ellipse.

^d Position angle of best-fit ellipse.

^e Rest-frame equivalent width of Ly α emission.

^f Flux within area given in column 4.

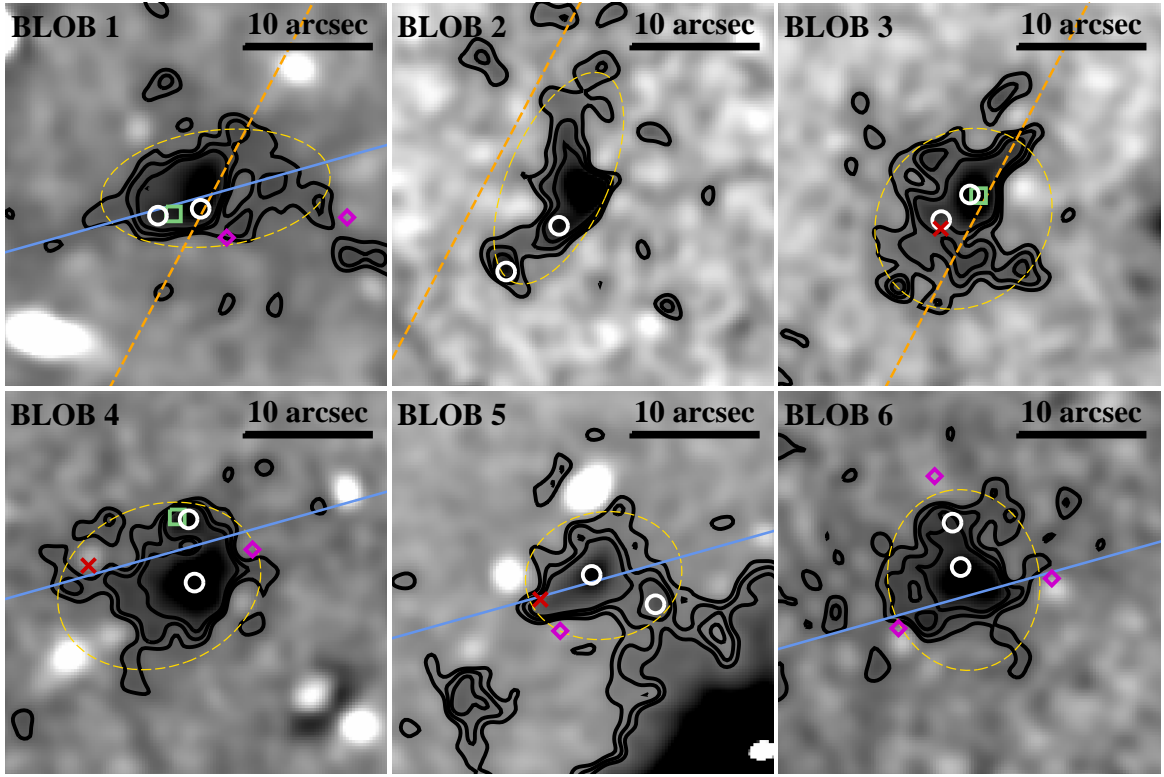


FIG. 1.— The six Ly α blobs are marked with contours on the smoothed, continuum-subtracted narrowband image. The contours are created after smoothing the image with a Gaussian of FWHM = 7 pixels ($\simeq 1.7''$), and are marked at surface brightness levels of 1.5 , 3 and 4.5×10^{-18} erg s⁻¹ cm⁻² arcsec⁻². Dashed yellow lines show ellipses fit to the largest 1.5×10^{-18} erg s⁻¹ cm⁻² arcsec⁻² contour. White circles show portions of the blobs classified as narrowband Ly α emitters, red crosses show UV continuum-selected galaxies spectroscopically confirmed to belong to the $z = 2.3$ protocluster, magenta diamonds show UV-selected $z \sim 2$ candidates with unknown redshifts, and green squares show DRGs whose redshifts are unknown (except the DRG associated with Blob 3, which has an absorption redshift associating it with the blob). The solid blue line is a least-squares fit to the positions of blobs 1, 4, 5 and 6 (also shown as the dashed line in Figure 2), and the dashed orange line is fit to the positions of blobs 1, 2 and 3 (also shown as the dot-dashed line in Figure 2). The images are oriented with north up and east to the left, and the scale bar in each window corresponds to 10 arcsec, or 82 proper kpc at $z = 2.3$. The bright object in the lower right corner of the image of blob 5 is a foreground star.

(Erb et al. 2006), and the IR-selected galaxy DRG38. DRG38 is coincident with a portion of the blob selected as a Ly α emitter, and followup spectroscopy reveals weak interstellar absorption lines with a redshift $z = 2.260$ as well as Ly α emission at $z = 2.290$. Ly α emission from the core of the blob is broad and multi-peaked, with $\sigma \sim 1400$ km s⁻¹.

Blob 4. This blob contains the IR-selected DRG72, with unknown redshift, and the UV-selected galaxy

BX909, a strong $24 \mu\text{m}$ source with $z_{\text{abs}} = 2.291$ and H α redshift $z = 2.2937$. An additional UV-selected source with unknown redshift, BX912, lies near the western edge of the blob. Spectroscopy of the two portions of the blob marked with white circles in Figure 1 yields Ly α redshifts of $z = 2.296$ at the core and $z = 2.288$ at the northern edge, for a velocity difference of ~ 700 km s⁻¹.

Blob 5. Blob 5 contains the UV-selected galaxy BX888, with $z_{\text{Ly}\alpha} = 2.270$ and $z_{\text{abs}} = 2.263$, and a UV-selected

galaxy of unknown redshift lies near the southern edge of the blob. As noted above, Blob 5 is at slightly lower redshift than the other blobs. The core of the blob shows a double-peaked Ly α emission line with $z = 2.267$ and $z = 2.272$, for a difference between the peaks of ~ 450 km s $^{-1}$. The spectrum may also show a weak C IV emission line. Blob 5 is not covered by IR imaging.

Blob 6. Blob 6 contains no galaxies with known redshifts, but three UV-selected $z \sim 2$ candidates lie just beyond the edges of the blob. Ly α emission is spatially extended with $z = 2.299$ and no velocity gradient. Blob 6 is not covered by IR imaging.

4. FILAMENTARY STRUCTURE AND BLOB ALIGNMENT

The six Ly α blobs span a region of approximately 12×6 comoving Mpc, and are distributed along two lines which intersect at the position of Blob 1 (see Figure 2; the edge of the narrowband image is just to the left of Blob 6, so the structure may extend farther to the east). Rest-frame UV-selected galaxies spectroscopically confirmed to be associated with the protocluster also tend to lie along and between these two lines, while narrowband-selected $z \sim 2.3$ Ly α emitters are more widely and randomly distributed.

The blobs therefore define two filamentary structures, viewed in projection. As noted in Section 3.2, the Ly α redshifts of the six blobs correspond to a velocity range of ~ 3700 km s $^{-1}$, with no correlation between position and redshift. Without systemic redshifts for the blobs, we cannot determine how much of these velocity differences are due to outflows or inflows within the blobs, relative velocities between the blobs, or real differences in physical distance.

We quantify the alignment of the blobs by fitting lines to the positions of Blobs 1, 4, 5 and 6, and to the positions of Blobs 1, 2 and 3. These two lines are shown in Figure 2, by the dashed and dot-dashed lines respectively. They are also shown in Figure 1, where the Blob 1-4-5-6 line (hereafter Line 1456) is shown in solid blue, and the Blob 1-2-3 line (hereafter Line 123) is dashed orange. Inspection of Figure 1 shows that these lines pass through or very close to all six blobs, the intersection of the two lines is at the center of Blob 1, and that all of the galaxies confirmed to be associated with the blobs, and all three of the DRGs, lie on or within only a few arcseconds of the lines.

We also compare the angles of these lines to the orientation of the blobs. Line 1456 is at an angle of 106° (measured east from north as usual), while the angle of Line 123 is 152° . We determine the position angle of each blob by fitting an ellipse to the largest contour at the 1.5×10^{-18} erg s $^{-1}$ cm $^{-2}$ arcsec $^{-2}$ flux level. The ellipses are shown by the dashed yellow lines in Figure 1, and the resulting angles are listed in Table 1. We find that the position angles of Blobs 1, 4, 5 and 6 are 97° , 110° , 100° and 9° respectively. With the exception of Blob 6, all of these blobs are aligned to within less than 10° along the line connecting them. Similarly, we measure position angles of 156° and 140° for Blobs 2 and 3 respectively, for offsets of 4° and 12° with respect to Line 123. Thus five of the six blobs are aligned to within $\sim 10^\circ$ of the lines connecting them. We also note that the position angle of Blob 6, the only blob that is misaligned, is significantly affected by the narrow extended

tail on the southwest edge of the blob; without this tail, the remainder of the blob is roughly aligned with Line 1456.

Given the nebulous, irregular borders of the blobs, the difficulty of reliably assigning an orientation, and the fact that only two show significant ellipticity $e \geq 0.5$, we should view this result with some caution. Nevertheless, the probability of the observed alignment happening by chance is extremely low. Assigning position angles at random to each of the six blobs and repeating the process 10^6 times, we find that at least five blobs are aligned to within 12° of the lines connecting them only 0.04% of the time. This suggests that the structure of the blobs is indeed related to the larger scale structure of which they are a part.

5. SUMMARY AND DISCUSSION

We have presented six ~ 100 kpc Ly α blobs in a protocluster at $z = 2.3$, the richest field of giant Ly α blobs detected to date. These blobs precisely define two intersecting filaments, much like the filaments along which galaxies form in cosmological simulations of structure formation (e.g. Springel et al. 2005). Moreover, we have shown that five of the six blobs are morphologically aligned with these filaments, indicating a connection between the processes responsible for Ly α emission in the blobs and the environment on larger scales.

Previous observations have firmly established the connection between Ly α blobs and environmental overdensities; as just one particularly relevant example, Matsuda et al. (2005) used a wide-field survey of Ly α emitters in the SSA22 field to establish the existence of large-scale filamentary structure at $z = 3.1$, and showed that the two giant Ly α blobs in that field are associated with those filaments, confirming the association of blobs with density peaks within overdense regions (Steidel et al. 2000). More recently, Matsuda et al. (2011) suggested a connection between the morphology of giant Ly α blobs and environment, finding that filamentary, elongated blobs reside in average density environments (as defined by the overdensity of Ly α emitters), while more circular blobs are found in both average and overdense regions. This observation leads to the hypothesis that circular blobs are associated with outflows from massive galaxies, while more filamentary blobs may be related to the accretion of cold gas from the IGM. The blobs presented here somewhat complicate this scenario, as they show a variety of morphologies from more to less elongated but are all found in relatively close proximity and in an overdense environment. On the other hand, the most elongated blob, Blob 2, is also the best candidate for emission arising from cold accretion, since it is the only one of the six blobs containing no UV or IR-selected galaxy candidates. Blob 2 also has the largest observed velocity gradient among the six, at ~ 1400 km s $^{-1}$ over 70 kpc, though this is difficult to interpret in terms of infall or outflow without systemic redshifts for the emitting regions.

The two new pieces this work brings to the picture are the nearly perfectly linear filaments on which the six $z = 2.3$ blobs fall, and the general alignment of the blobs with those structures. Perhaps the most obvious interpretation of this result is that at least some of the Ly α emission from the blobs arises from gas falling

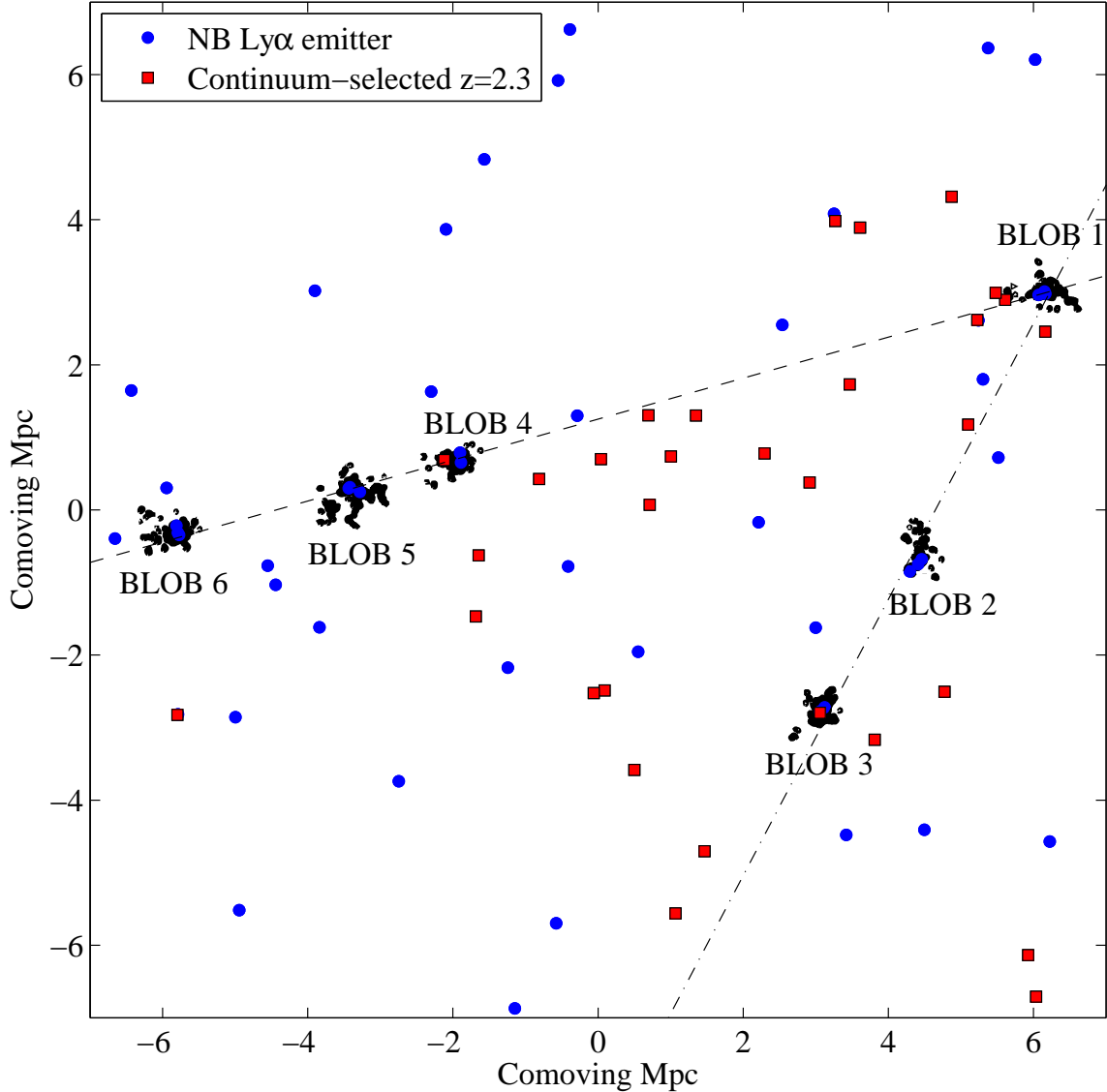


FIG. 2.— The six Ly α blobs, NB-selected Ly α emitters, and rest-frame UV continuum-selected members of the $z = 2.3$ protocluster. The dashed line is a least-squares fit to the positions of blobs 1, 4, 5 and 6, and the dot-dashed line is a fit to the positions of blobs 1, 2 and 3.

into massive galaxies forming along the filaments. This may be a reasonable conclusion; although recent simulations suggest that emission from cold accretion is insufficient to entirely power the large Ly α blobs, it may play an important role even if not energetically dominant (Faucher-Giguère et al. 2010). However, most of the blobs have galaxies associated with them, and three of those galaxies are IR-selected DRGs; the DRGs are likely to be massive, and given their low surface density, their association with the blobs is unlikely to be coincidental. This fact, coupled with the large spatial and velocity extent of gas outflowing from galaxies and the ability of Ly α photons from within the galaxies to resonantly scatter in that gas (Steidel et al. 2010, 2011; Zheng et al. 2010), suggests that heating from within is also likely to be a significant power source for the blobs. Resonant scattering may also result in Ly α emission from filamentary gas around galaxies whether or not the gas is accreting, complicating the relationship between blob power sources and morphologies.

The Ly α blobs in the HS 1700+64 protocluster suggest a complex interplay between outflowing and infalling gas, mediated by the resonant scattering of Ly α photons which couples the emission from galaxies to the environment on larger scales. We look forward to much deeper narrowband images of this region, when the technology becomes available; such images will likely reveal more extended Ly α emission, possibly further tracing the filamentary structures identified by the blobs. Additional observations will also more thoroughly reveal the velocity structure of the blobs, for better constraints on their emission mechanisms and on the complex processes of radiative transfer which produce them.

Alice Shapley, Naveen Reddy and Max Pettini provided essential contributions to the survey on which this work is based. We also thank the staffs of Palomar and Keck Observatories for assistance with the observations, Yuichi Matsuda for useful suggestions, and the ref-

eree for helpful comments. D.K.E. acknowledges support from the University of Wisconsin Research Growth Initiative, and C.C.S. from the US National Science Founda-

tion through grants AST-0606912 and AST-0908805, with additional support from the John D. and Catherine T. MacArthur Foundation and the Peter and Patricia Gruber Foundation.

REFERENCES

- Barmby, P., Huang, J.-S., Fazio, G. G., Surace, J. A., Arendt, R. G., Hora, J. L., Pahre, M. A., Adelberger, K. L., Eisenhardt, P., Erb, D. K., Pettini, M., Reach, W. T., Reddy, N. A., Shapley, A. E., Steidel, C. C., Stern, D., Wang, Z., & Willner, S. P. 2004, *ApJS*, 154, 97
- Colbert, J. W., Scarlata, C., Teplitz, H., Francis, P., Palunas, P., Williger, G. M., & Woodgate, B. 2011, *ApJ*, 728, 59
- Digby-North, J. A., Nandra, K., Laird, E. S., Steidel, C. C., Georgakakis, A., Bogosavljević, M., Erb, D. K., Shapley, A. E., Reddy, N. A., & Aird, J. 2010, *MNRAS*, 407, 846
- Dijkstra, M. & Loeb, A. 2009, *MNRAS*, 400, 1109
- Erb, D. K., Steidel, C. C., Shapley, A. E., Pettini, M., Reddy, N. A., & Adelberger, K. L. 2006, *ApJ*, 646, 107
- Faucher-Giguère, C.-A., Kereš, D., Dijkstra, M., Hernquist, L., & Zaldarriaga, M. 2010, *ApJ*, 725, 633
- Franx, M., Labbé, I., Rudnick, G., van Dokkum, P. G., Daddi, E., Förster Schreiber, N. M., Moorwood, A., Rix, H., Röttgering, H., van de Wel, A., van der Werf, P., & van Starkenburg, L. 2003, *ApJ*, 587, L79
- Geach, J. E., Alexander, D. M., Lehmer, B. D., Smail, I., Matsuda, Y., Chapman, S. C., Scharf, C. A., Ivison, R. J., Volonteri, M., Yamada, T., Blain, A. W., Bower, R. G., Bauer, F. E., & Basu-Zych, A. 2009, *ApJ*, 700, 1
- Goerdt, T., Dekel, A., Sternberg, A., Ceverino, D., Teyssier, R., & Primack, J. R. 2010, *MNRAS*, 407, 613
- Haiman, Z., Spaans, M., & Quataert, E. 2000, *ApJ*, 537, L5
- Keel, W. C., White, III, R. E., Chapman, S., & Windhorst, R. A. 2009, *AJ*, 138, 986
- Kriek, M., van Dokkum, P. G., Franx, M., Illingworth, G. D., & Magee, D. K. 2009, *ApJ*, 705, L71
- Matsuda, Y., Nakamura, Y., Morimoto, N., Smail, I., De Breuck, C., Ohta, K., Kodama, T., Inoue, A. K., Hayashino, T., Kousai, K., Nakamura, E., Horie, M., Yamada, T., Kitamura, M., Saito, T., Taniguchi, Y., Tanaka, I., & Hibon, P. 2009, *MNRAS*, 400, L66
- Matsuda, Y., Yamada, T., Hayashino, T., Tamura, H., Yamauchi, R., Ajiki, M., Fujita, S. S., Murayama, T., Nagao, T., Ohta, K., Okamura, S., Ouchi, M., Shimasaku, K., Shioya, Y., & Taniguchi, Y. 2004, *AJ*, 128, 569
- Matsuda, Y., Yamada, T., Hayashino, T., Tamura, H., Yamauchi, R., Murayama, T., Nagao, T., Ohta, K., Okamura, S., Ouchi, M., Shimasaku, K., Shioya, Y., & Taniguchi, Y. 2005, *ApJ*, 634, L125
- Matsuda, Y., Yamada, T., Hayashino, T., Yamauchi, R., Nakamura, Y., Morimoto, N., Ouchi, M., Ono, Y., Kousai, K., Nakamura, E., Horie, M., Fujii, T., Umemura, M., & Mori, M. 2011, *MNRAS*, 410, L13
- McCarthy, P. J., Spinrad, H., Djorgovski, S., Strauss, M. A., van Breugel, W., & Liebert, J. 1987, *ApJ*, 319, L39
- Nilsson, K. K., Fynbo, J. P. U., Møller, P., Sommer-Larsen, J., & Ledoux, C. 2006, *A&A*, 452, L23
- Palunas, P., Teplitz, H. I., Francis, P. J., Williger, G. M., & Woodgate, B. E. 2004, *ApJ*, 602, 545
- Peter, A. H. G., Shapley, A. E., Law, D. R., Steidel, C. C., Erb, D. K., Reddy, N. A., & Pettini, M. 2007, *ApJ*, 668, 23
- Prescott, M. K. M., Kashikawa, N., Dey, A., & Matsuda, Y. 2008, *ApJ*, 678, L77
- Reddy, N. A., Erb, D. K., Pettini, M., Steidel, C. C., & Shapley, A. E. 2010, *ApJ*, 712, 1070
- Reddy, N. A., Erb, D. K., Steidel, C. C., Shapley, A. E., Adelberger, K. L., & Pettini, M. 2005, *ApJ*, 633, 748
- Shapley, A. E., Steidel, C. C., Erb, D. K., Reddy, N. A., Adelberger, K. L., Pettini, M., Barmby, P., & Huang, J. 2005, *ApJ*, 626, 698
- Smith, D. J. B., Jarvis, M. J., Lacy, M., & Martínez-Sansigre, A. 2008, *MNRAS*, 389, 799
- Springel, V., White, S. D. M., Jenkins, A., Frenk, C. S., Yoshida, N., Gao, L., Navarro, J., Thacker, R., Croton, D., Helly, J., Peacock, J. A., Cole, S., Thomas, P., Couchman, H., Evrard, A., Colberg, J., & Pearce, F. 2005, *Nature*, 435, 629
- Steidel, C. C., Adelberger, K. L., Shapley, A. E., Erb, D. K., Reddy, N. A., & Pettini, M. 2005, *ApJ*, 626, 44
- Steidel, C. C., Adelberger, K. L., Shapley, A. E., Pettini, M., Dickinson, M., & Giavalisco, M. 2000, *ApJ*, 532, 170
- Steidel, C. C., Bogosavljević, M., Shapley, A. E., Kollmeier, J. A., Reddy, N. A., Erb, D. K., & Pettini, M. 2011, *ApJ*, 736, 160
- Steidel, C. C., Erb, D. K., Shapley, A. E., Pettini, M., Reddy, N., Bogosavljević, M., Rudie, G. C., & Rakic, O. 2010, *ApJ*, 717, 289
- Steidel, C. C., Shapley, A. E., Pettini, M., Adelberger, K. L., Erb, D. K., Reddy, N. A., & Hunt, M. P. 2004, *ApJ*, 604, 534
- Taniguchi, Y. & Shioya, Y. 2000, *ApJ*, 532, L13
- Wuyts, S., van Dokkum, P. G., Franx, M., Förster Schreiber, N. M., Illingworth, G. D., Labbé, I., & Rudnick, G. 2009, *ApJ*, 706, 885
- Yang, Y., Zabludoff, A., Tremonti, C., Eisenstein, D., & Davé, R. 2009, *ApJ*, 693, 1579
- Zheng, Z., Cen, R., Weinberg, D., Trac, H., & Miralda-Escude, J. 2010, *arXiv:1010.3017*